Chapter 4

Tunneling and the semiclassical propagator

4.1 A quantum-semiclassical approach

4.1.1 Motivation

In the foregoing Chapter 3, tunneling was described in the energy domain by means of classical trajectories with imaginary or complex momenta. The present Chapter addresses the question whether tunneling may be described in the time domain by means of the semiclassical propagator (cf. Section 2.3.2),

$$K^{(\mathrm{sc})}(\mathbf{q}, \mathbf{q}_0; t) = \sum_j A_j \, e^{iS_j/\hbar}, \tag{4.1}$$

where A_j is given by the prefactor of the r.h.s. of Eq. (2.83) multiplied by the phase factor $e^{-\phi}$. The sum over individual trajectories that connect $\mathbf{q}_0$ and $\mathbf{q}$ by a trajectory with propagation time t is explicitly included. In particular, these classical trajectories have real positions *and* momenta.

The present work is concerned with bound systems. Autocorrelation functions, $C(t) = \langle \Psi | e^{-i\hat{H}t/\hbar} | \Psi \rangle$, of bound system with time-independent Hamiltonians can be expressed as

$$C(t) = \sum_\nu d_\nu \, \exp\{-i\omega_\nu t\}, \tag{4.2}$$

where $d_\nu = |\langle \nu | \Psi \rangle|^2$ are the absolute squares of the expansion coefficients of $|\Psi\rangle$ in terms of eigenstates $|\nu\rangle$. The Fourier transformation of $C(t)$ yields an energy spectrum $I(\omega)$. The semiclassical approximation to $C(t)$ is given by

$$C^{(\mathrm{sc})}(t) = \int_{-\infty}^{\infty} dq \int_{-\infty}^{\infty} dq_0 \, \Psi^*(q) \, K^{(\mathrm{sc})}(q, q_0; t) \, \Psi(q_0). \tag{4.3}$$
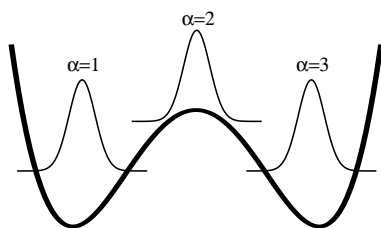
Figure 4.1: Illustration of the quantum-semiclassical approach. Three Gaussians $|\Psi_\alpha\rangle$ are distributed over the x-range of a double-well PES.

Fourier transformation of this autocorrelation function yields a semiclassical spectrum $I^{(\mathrm{sc})}(\omega)$ leading to an alternative method for semiclassical quantization (cf. Section 2.1.5). Unlike adiabatic switching, such method does not rely on the existence of invariant tori [130]. Instead of the van Vleck propagator [Eq. (4.1)] one may also use the Herman-Kluk propagator (cf. Sec. 2.3.2). The corresponding quantities are referred to as $C^{(HK)}(t)$ and $I^{(HK)}(\omega)$.

Previously, Sun and Miller [92] obtained low lying vibrational levels of the HCl dimer by computing $I^{(HK)}(\omega)$. In particular, the ground state tunneling splitting was obtained. Since only real-valued trajectories appear in the HK propagator, these tunneling splittings are given in terms of over-barrier trajectories [131]. It was shown, however, that semiclassical tunneling probabilities depend upon unphysical parameters [132, 133, 134]. For instance, Kay [134] demonstrated dependence upon a width parameter γ that is related to the corresponding HK parameter (cf. Section 2.3.2). Moreover, the semiclassical error increases with the propagation time [131]. Subject of the remaining part of this Section is a proposed means to overcome the considered deficiencies of the alternative semiclassical quantization technique.

4.1.2 Quantization by harmonic inversion

Instead of Fourier transforming single auto-correlation functions, it was suggested [36, 130, 135] to analyze $L \times L$ cross-correlation functions,

$$C_{\alpha\alpha'}^{(\mathrm{sc})}(t) = \langle \Psi_\alpha | \hat{K}^{(\mathrm{sc})}(t) | \Psi_{\alpha'} \rangle, \tag{4.4}$$

where $\hat{K}^{(\mathrm{sc})}(t)$ is a semiclassical propagator and $|\Psi_\alpha\rangle$ with $1 \leq \alpha \leq L$ are initial wave packets, by *harmonic inversion*. The harmonic inversion of $C_{\alpha\alpha'}^{(\mathrm{sc})}(t)$ is the solution to the non-linear fitting problem,

$$C_{\alpha\alpha'}^{(\mathrm{sc})}(t) = \sum_\nu d_{\nu,\alpha\alpha'} \exp\{-i\omega_\nu t\}, \tag{4.5}$$

where $\{d_{\nu,\alpha\alpha'}, \omega_\nu\}$ generally are complex fit parameters. While harmonic inversion is a well-defined problem for a quantum propagator, the ansatz Eq. (4.5) is based on the assumption, that the semiclassical time evolution – for short times –

can be expressed by a propagator $\exp\{-i\hat{H}_{\mathrm{eff}}t/\hbar\}$ with an effective Hamiltonian $\hat{H}_{\mathrm{eff}}$ [130, 39]. For instance, Section 2.3.2 showed for the 1D HK propagator that such an effective Hamiltonian comes out as the linear term of a Taylor expansion with respect to time. A similar situation is assumed for the multidimensional case without proof. However, in order to pose a sound harmonic inversion problem, it is necessary to account for deviations of $\hat{H}_{\mathrm{eff}}$ from hermiticity by allowing ω_ν to be complex-valued [37, 38]. Moreover, in order to simplify the discussion all initial wave packets are assumed to be real. (This is without loss of generality for time-independent real Hamiltonians.)

A means for numerical solution of Eq. (4.5) for a given interval $[\omega_{\mathrm{min}}, \omega_{\mathrm{max}}]$ is the *Filter Diagonalization Method* (FDM) by Wall and Neuhauser [136] that was improved by Mandelshtam and Taylor [37] (see Ref. [38] for a recent review). The derivation of the method is subject of Section 4.1.3. The advantage of FDM compared to a Fourier transformation is expressed by the *informational uncertainty principle* [37]: if $\bar{\omega}$ is the mean level spacing in $[\omega_{\mathrm{min}}, \omega_{\mathrm{max}}]$ and the L wave packets are sufficiently linear-independent, then the levels in that interval can be determined provided that the propagation time T satisfies,

$$\frac{T}{2} \geq \frac{1}{L}\frac{2\pi}{\bar{\omega}}. \tag{4.6}$$

Especially, when there are near degenerate levels (e.g., tunnel doublets) the mean level spacing $\bar{\omega}$ is much larger than the minimal level spacing $\Delta\omega_{\mathrm{m}}$. Therefore, FDM requires typically a much smaller propagation time as a Fourier transform, where the propagation time has to exceed $2\pi/\Delta\omega_m$ in order to resolve all levels. Moreover, by increasing L the propagation time can be reduced further. Therefore, only a comparatively short time interval is necessary for harmonic inversion of $C_{\alpha\alpha'}(t)$, which makes the method well suited for semiclassical quantization. (Recall, the semiclassical error increases with time.)

A limiting case of the FDM applied to cross-correlation functions is the choice of a complete basis set $\{|\Psi_\alpha\rangle\}$ for the initial wave functions [36]. Then, as is shown in Section 4.1.3, the FDM corresponds to a diagonalization of the Hamiltonian matrix $\langle\Psi_\alpha|\hat{H}_{\mathrm{eff},0}|\Psi_{\alpha'}\rangle$, where the effective Hamiltonian at $t = 0$ is tentatively defined as $i\hbar\partial\hat{K}^{(\mathrm{sc})}(t)/\partial t|_{t=0} \equiv \hat{H}_{\mathrm{eff},0}$. Another limit results for a harmonic PES, where the semiclassical cross-correlation function is exact. This motivates a hybrid quantum-semiclassical approach for the treatment of multidimensional systems. It was suggested [36] that the choice of an intermediate L introduces *quantum information* into a semiclassical propagation. For instance, consider the SMC PES Fig. 2.7 (top). One can distribute initial wave packets along the x-axis in order to "diagonalize" that DOF while the harmonic PES along the q-axis (for each fixed x) is exactly accounted for by the semiclassical propagator.

Tunneling splittings were extracted by the quantum semiclassical approach for one and two-dimensional model PES [39]. However, it is shown in this work [II][1], that the idea of introducing quantum information into a semiclassical propagation is unsound. The reason is that the initial effective Hamiltonian $\hat{H}_{\text{eff},0}$ is different from the exact quantum Hamiltonian $\hat{H}$. Thus, whether quantum effects are accounted for by the quantum semiclassical approach depends on whether these effects are present in the initial effective Hamiltonian.

4.1.3 Filter diagonalization method for cross-correlation functions

The FDM is a means to solve the non-linear fitting problem Eq. (4.5) [136, 137, 37, 38]. Here, the version of Mandelshtam and Taylor [137, 37, 38] is used because it showed a reasonable accuracy even when the propagation time was quite at the limit of convergence for some model systems [138]. The idea is to recast the non-linear fitting problem posed by Eq. (4.5) into a linear one. The method proceeds as follows:

1. Select J frequencies ϕ_j ($j = 1, \ldots, J$) equidistantly spaced in the interval $[\omega_{\min}, \omega_{\max}]$ with,

$$J = N\tau(\omega_{\max} - \omega_{\min})/4\pi, \tag{4.7}$$

   where τ is the discrete step size and $T = N\tau$ is the total propagation time.

2. Define a *Krylov* base with $M = (N-2)/2$ by:

$$|\Psi_\alpha(\phi_j)\rangle = \sum_{n=0}^{M} \exp\{in\tau\phi_j\}|\Psi_\alpha(n\tau)\rangle, \tag{4.8}$$

   where wave functions are distinguished by their argument (either time or frequency).

3. Solve the generalized eigenvalue problem,

$$\mathbf{U}^p\mathbf{B} = \lambda\mathbf{U}^0\mathbf{B}, \tag{4.9}$$

   where $p \neq 0$ is an integer, $\mathbf{B}$ are the eigenvectors, and $\lambda = \exp\{-i\omega p\tau\}$ are the eigenvalues. The matrix elements read

$$U^p_{\alpha j,\alpha' j'} = \langle\Psi_\alpha(\phi_j)|\hat{K}(p\tau)|\Psi_{\alpha'}(\phi_{j'})\rangle. \tag{4.10}$$

   The integer p is necessary in order to detect spurious eigenvalues; the issue is detailed below.

---

[1]paper (II) of the publication list

The propagated wave packets can be expressed in terms of the eigenstates $|\varphi_\nu\rangle$ and eigenenergies $\hbar\omega_\nu$ of the corresponding Hamiltonian $\hat{H}$. In the case of a semiclassical propagation, the ω_ν may also be complex. Inserting the expansion with expansion coefficients a_ν into Eq. (4.8) unveils,

$$|\Psi_\alpha(\phi_j)\rangle = \sum_\nu a_\nu\, F(\phi_j - \omega_\nu)\, |\nu\rangle, \tag{4.11}$$

with

$$F(\delta) = \sum_{n=0}^{M} \exp\{in\tau\delta\} = \frac{1 - e^{i\tau\delta(M+1)}}{1 - e^{i\tau\delta}}, \tag{4.12}$$

i.e., the contribution of each eigenfunction is weighted by a function $F(\phi_j - \omega_\nu)$. This function has a main maximum at $\phi_j = \omega_m$ ($\delta = 0$) with $\lim_{\delta\to 0}|F(\delta)| = M + 1$ and many considerably lower submaxima. The first subminimum is at $\tau\delta\,(M+1) = 2\pi$. Together with the definition of N ($N/2 = M+1$) and $T = N\tau$ this yields: $T/2 = 2\pi/\delta$. Let $\bar{\omega}$ be the mean level spacing in the interval $[\omega_{\min}, \omega_{\max}]$, then, if $\delta < \bar{\omega}$, each basis function $|\Psi_\alpha(\phi_j)\rangle$ picks out approximately one eigenfunction. This is the informational uncertainty principle [cf. Eq. (4.6)] for $L = 1$. It suggests that for a single initial wavepacket $L = 1$ and propagation times that satisfy the relation, $T/2 \geq 2\pi/\bar{\omega}$, the solution of the generalized eigenvalue problem Eq. (4.9) will yield all eigenvalues in the interval $[\omega_{\min}, \omega_{\max}]$. Loosely speaking, the eigenvalue problem converges. However, according to its derivation, the principle is only a rule of thumb.

The propagation time can be reduced by using more initial wave packets $L > 1$. Assuming, that the L Krylov vectors $|\Psi_\alpha(\phi_j)\rangle$ belonging to a certain ϕ_j are linearly independent, one would expect, that these vectors form a base for diagonalizing at most L eigenfunction in the interval δ. This leads to the informational uncertainty principle Eq. (4.6) for arbitrary L.

The numerical solution of the generalized eigenvalue problem Eq. (4.9) is hampered by the fact, that in general the Krylov base function are linearly dependent. This leads to spurious eigenvalues. Part of the spurious eigenvalues can be removed by *singular value decomposition* (SVD) [136], i.e., eigenvalues of $\mathbf{U}^0$ below a certain threshold are neglected. In this work a relative threshold, denoted as R_{TOL}, was used; all eigenvalues below R_{TOL} times the maximum eigenvalue are removed. An alternative way to solve the generalized eigenvalue problem is to resort to *regularization* [139, 38].

SVD (or regularization) cannot remove all spurious eigenvalues. Another sign of a spurious eigenvalue in a bound system is a large imaginary part. Moreover, spurious eigenvalues can be identified by solving the generalized eigenvalue problem Eq. (4.9) for different values of the integer p [37]. Additionally, in this work eigenvalues are neglected if (i) the absolute difference of $p = 1$ and $p = 2$ values

exceeds the threshold E_{TOL} or (ii) the imaginary part is larger than I_{TOL} times the absolute value of the real part. This still does not remove all spurious eigenvalues. However, for a plot of ω vs. propagation time T the "good" eigenvalues are on a line while the spurious eigenvalues are erratically scattered (see below).

4.2 Numerical investigation of the quantum-semiclassical approach

4.2.1 The square quartic Hamiltonian

The objective of this Section is a numerical and analytical analysis of the quantum-semiclassical approach suggested in Ref. [36]. To this end, the square-quartic Hamiltonian (in recast form; cf. Sec. 3.3.1),

$$\hat{H} = -\frac{g^2}{2}\frac{\partial^2}{\partial x^2} + \tilde{V}_0\left(x^4 - 2x^2 + 1\right), \quad \tilde{V}_0 = \frac{1}{8}, \qquad (4.13)$$

was used as model system. (This form was chosen, because it depends only on one parameter.) The eigenstates $|\varphi_\nu^\pm\rangle$ and eigenlevels $\omega_\nu^\pm$ can be characterized by their symmetry as gerade (+) and ungerade (-). According to Section 2.3.2, the HK error operator at $t = 0$ of this Hamiltonian (with HK parameter γ),

$$\hat{F}_0 = -\tilde{V}_0\frac{3}{4}\gamma^{-2} \equiv -\delta, \qquad (4.14)$$

is a constant [II]. Thus, for short times, the HK propagation is governed by the Hamiltonian $\hat{H}' = \hat{H} - \delta$ [cf. Eq. (2.94)]. The eigenstates of $\hat{H}$ and $\hat{H}'$ are identical, while the eigenlevels of $\hat{H}'$ are shifted by $-\delta$. Therefore, harmonic inversion of any cross-correlation function $C_{\alpha\alpha'}(t)$ yields shifted eigenlevels $\omega_n^\pm - \delta$ as long as the $\mathcal{O}(t^2)$ error is small enough. Surprisingly, this means, that a propagation based on pure real-valued classical trajectories yields eigenlevels that are split due to tunneling. Note, this finding is an exact result.

For a practical application it is necessary to know how small t must be in order to be able to determine eigenlevels. Here, the determination of tunneling splittings is of special interest because they are strongly affected by the semiclassical error. To be definite, two parameters of g were considered. The six lowest eigenlevels of the corresponding models are shown in Tab. 4.1 (obtained by numerical exact diagonalization). Model A with $g = 0.09$ has two levels below the barrier. The magnitude of the ground state tunneling splitting of this model was rather at the limit of being determined with the present technique. Model B with $g = 0.17$ is intermediate between Model A and the case with no level below the barrier. For a harmonic frequency Ω_x [cf. Eq. (3.18)] at the minimum of $3000\,\mathrm{cm}^{-1}$

	(A) $g = 0.09$		(B) $g = 0.17$	
	exact	gauss	exact	gauss
ω_0^+	0.3402	0.3402	0.5587	0.5588
ω_0^-	0.3430	0.3430	0.6583	0.6584
ω_1^+	0.8823	0.8824	1.4270	1.4276
ω_1^-	0.9724	0.9724	2.0452	2.0469
ω_2^+	1.3154	1.3159	2.8717	2.8805
ω_2^-	1.6261	1.6270	3.7939	3.8153

Table 4.1: Eigenvalues (in units of the dimensionless barrier height $\tilde{V}_0 = 1/8$) for the one-dimensional square-quartic Hamiltonian [cf. Eq. (4.13)] with dimensionless parameter $g = 0.09$ (Model A) and parameter $g = 0.17$ (Model B). Numerically exact ('exact') and approximate values ('gauss') are given (see text).

(typical for OH stretch) the barrier heights corresponding to model A and B are, respectively, $4167\,\mathrm{cm}^{-1}$ and $2206\,\mathrm{cm}^{-1}$. (For comparison: for a 2D SMC model of malonaldehyde g was 0.10.)

As initial wave packets a set $\{|\Psi_\alpha\rangle\}$ of $L = 14$ Gaussians equidistantly spaced in the interval $[-1.2, 1.2]$ was chosen. The momenta were zero and the width was $\gamma_\alpha = 12.5$. The set is sufficient to diagonalize the below barrier levels of both models; eigenlevels obtained from the solution of the corresponding generalized eigenvalue problem are also given in Tab. 4.1. The formally arbitrary parameter γ of the HK propagator was chosen to equal 12.5 (cf., for instance, Ref. [94]). The trajectory sampling method was discussed in Section 2.3.2; $5 \cdot 10^5$ trajectories were sampled for the propagation of each single wave packet. A fifth-order symplectic integrator [116] with fixed step size τ typically $10^{-3}\,T^*$ was used. The characteristic time $T^* = 2\pi/g$ was defined in Sec. 3.3.1. Plots of $\mathrm{Re}\,\omega_\nu$ vs. propagation time T obtained from harmonic inversion by FDM of the HK propagated cross-correlation function $C_{\alpha\alpha'}(t)$ were investigated. The choice of the set $\{|\Psi_\alpha\rangle\}$ ensured that the FDM converges rapidly.

Figure 4.2 shows results obtained for both models, A and B. The exact levels are indicated by straight lines. The semiclassical error manifests itself by a deviations of $\mathrm{Re}\,\omega_\nu$ from the exact value and by the appearance of spurious levels. For both systems the number of spurious eigenvalues increases with time because of the increasing noise. A value of $R_{\mathrm{TOL}} = 10^{-4}$ was necessary to get reasonable results in the semiclassical calculations. System A (cf. Fig 4.2a and b) has two split levels below the barrier. Fig. 4.2b shows the lowest split level, $0+$ and $0-$, of system A in more detail. From Fig. 4.2b it is clear that the small splitting of
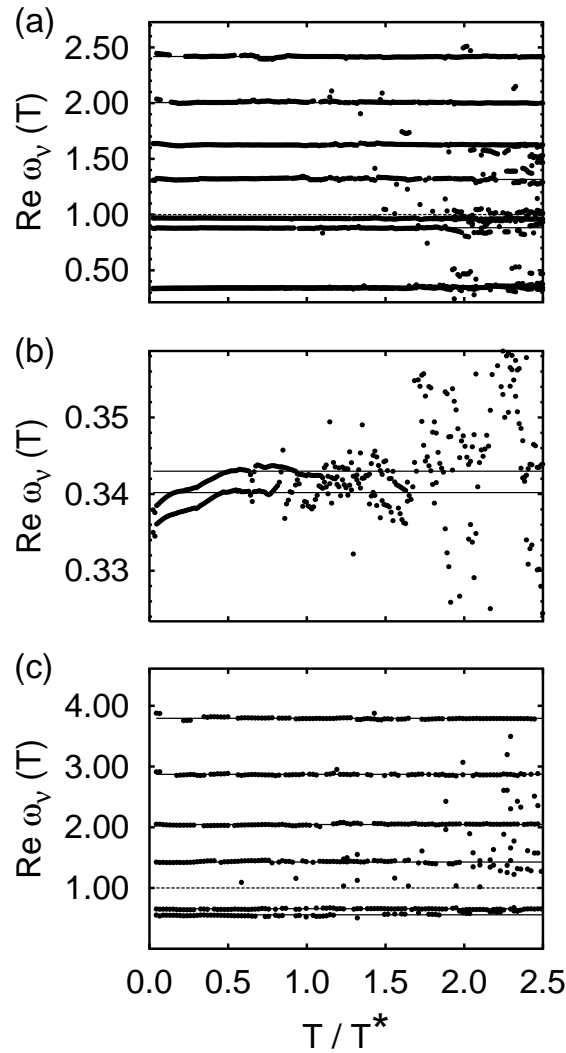
Figure 4.2: One-dimensional Hamiltonian Eq. (4.13): Frequencies $\omega_\nu(T)$ in units of the barrier height vs. propagation time T in units of T^* obtained by harmonic inversion of the 14×14 HK-propagated cross-correlation matrix. (a) model A ($g = 0.09$), (b) model A (enlarged), and (c) model B ($g = 0.17$). Solid lines indicate the exact energy levels and the dashed line indicates the barrier. The FDM parameters (cf. Section 4.1.3) are $J = 5$, $\omega_{\text{center}} = 1.0$ (the center of the energy window), $R_{\text{TOL}} = 10^{-4}$, $E_{\text{TOL}} = 1.5 \cdot 10^{-3}$, $I_{\text{TOL}} = 5 \cdot 10^{-2}$.

the lowest level can only be obtained until $0.5T^*$, whereas the first excited state splitting (cf. Fig. 4.2a) is almost exact for times up to about $1.8T^*$. Several higher levels can be resolved for an even longer time.

In model B the situation is qualitatively equivalent to model A. The splitting of the levels below the barrier can be obtained for about $1T^*$ to $1.5T^*$. Most higher levels can be obtained even within a longer interval. Thus, for the present choice of initial Gaussians and the HK-parameter γ, the tunneling splitting can be obtained for few characteristic periods in the present models resembling a reasonable range of parameters g. In all cases the splitting was obtained for $T \approx 0$, since it is present in the level structure of the effective Hamiltonian as was shown analytically.

It is important to note that the reason why it is possible to obtain tunneling splittings from semiclassical correlation functions is *not* related to the choice of the diagonalizing basis set. Implicitly, this was shown already because the HK propagation for short times is governed exactly by the Hamiltonian $\hat{H}'$ that deviates from the exact Hamiltonian $\hat{H}$ only by the constant δ. However, since it is somewhat against intuition, a more direct evidence is appreciable. To this end, consider a *single* initial wave packet $|\Psi\rangle$ propagated according to the HK propagator (propagation parameters as before). At any instant of time t it is possible to express the time evolved wavepacket $|\Psi\rangle_t$ in terms of the *exact* eigenfunctions $|\varphi_\nu^\pm\rangle$ as:

$$\begin{aligned} |\Psi\rangle_t &= \sum_\nu a_\nu^+ \exp\{-i\beta_\nu^+(t)\} |\varphi_\nu^+\rangle \\ &+ \sum_\nu a_\nu^- \exp\{-i\beta_\nu^-(t)\} |\varphi_\nu^-\rangle, \end{aligned} \qquad (4.15)$$

with $a_\nu^\pm = \langle\varphi_\nu^\pm|\Psi\rangle$ and complex time-dependent phases $\beta_\nu^\pm(t)$. For an exact quantum propagation one would have $\beta_\nu^\pm(t) = \omega_\nu^\pm t$, where $\omega_\nu^\pm$ are the exact eigenvalues of the Hamiltonian Eq. (4.13). The semiclassical error of the HK propagation will manifest itself especially for phase differences $\sigma(t) = \beta_\nu^-(t) - \beta_\nu^+(t)$ of state pairs, that are split by tunneling. These phase differences are given by the logarithm of the normalized expectation value of $\hat{P} \equiv |\varphi_\nu^-\rangle\langle\varphi_\nu^+|$ (times $-i$) [II]:

$$\sigma(t) = -i \ln \frac{{}_t\langle\Psi|\hat{P}|\Psi\rangle_t}{\langle\Psi|\hat{P}|\Psi\rangle}. \qquad (4.16)$$

According to Eq. (2.94) it follows that $\sigma(t) = \Delta\omega_\nu t + \mathcal{O}(t^2)$, where $\Delta\omega_\nu$ is the exact tunneling splitting.

The relation for $\sigma(t)$ was investigated for the two models and individual Gaussians out of the set $\{|\Psi_\alpha\rangle\}$. The eigenstates $|\varphi_\nu^\pm\rangle$ of the below barrier levels can be expressed in terms of the set of $L = 14$ Gaussians as,

$$|\varphi_\nu^\pm\rangle = \sum_\alpha c_{\nu\alpha}^\pm |\Psi_\alpha\rangle, \qquad (4.17)$$

where $c_{\nu\alpha}^{\pm}$ are the corresponding expansion coefficients. Using this equation the expectation value of $\hat{P}$ can be expressed as,

$$_t\langle\Psi_\beta|\hat{P}|\Psi_\beta\rangle_t = \sum_{\alpha,\alpha'} \left(c_{\nu\alpha}^+\right)^* c_{\nu\alpha'}^- C_{\alpha'\beta}^*(t)\, C_{\alpha\beta}(t),$$ (4.18)

where $|\Psi_\beta\rangle$ is an individual Gaussian out of the set $\{|\Psi_\alpha\rangle\}$. Thus, the expectation value only depends on a single *column* of the cross-correlation function, i.e., only the propagation of a single Gaussian contributes.

The plot of $\mathrm{Re}\,\sigma(t)$ for the lowest levels $0+$ and $0-$ of model A in Fig. 4.3a shows, that the behavior of $\sigma(t)$ depends on the initial position of the Gaussian. The results for the first four Gaussians exhibit an approximately linear increase until roughly $1.0T^*$; for longer time the deviations from linearity become very prominent. The last Gaussian with position $x = 0.09$ already deviates very strongly from linear increase for $0.5T^*$.

For the excited pair of levels, $1+$ and $1-$, of model A the findings are similar (cf. Fig. 4.3b). Most Gaussians show an approximately linear increase for times up to $1.0T^*$ and deviations for longer time. The Gaussian with initial position $x = 0.83$ deviates considerably already for $0.5T^*$ from the exact linear increase.

The plot of $\mathrm{Re}\,\sigma(t)$ of the lowest levels $0+$ and $0-$ of model B (cf. Fig. 4.3c) shows linear increase with time up to roughly time $1.0T^*$ for most Gaussians; the Gaussian with $x = 0.09$ deviates most rapidly from linear increase for times larger then $0.8T^*$.

To summarize: In all cases $\mathrm{Re}\,\sigma(t)$ deviates very strongly from linear increase for times larger then T^*. However, since each curve in Fig. 4.3 is obtained for a *single* HK-propagated Gaussian, the linearity for short times supports the statement, that the spectrum of $\hat{H}'$ includes the levels below the barriers in *split* pairs. For time $t = 0$ this was already shown analytically above. The strong deviations from linear behavior for times $t > T^*$ clearly show that the eigenfunctions of $\hat{H}'$ differ considerably from the exact eigenfunctions. The nature of this deviation cannot be deduced from the present numerical calculation: there may be an overall shift of the eigenvalues still being split due to tunneling. If the magnitude of the splitting or the mean of the pair of split eigenvalues is shifted substantially for times $t > T^*$, one would expect a decrease in accuracy when applying harmonic inversion, since in its derivation a time independent Hamiltonian $\hat{H}_{\mathrm{eff}}$ was assumed. From the viewpoint of FDM this *moving* frequencies look like noise; but in contrast to white noise the kind of noise introduced by the HK-propagator is a *systematic* deviation.

Note that there is no simple relation between Gaussian parameters and the deviation from the exact behavior. For instance, in Fig. 4.3a and 4.3c the Gaussians
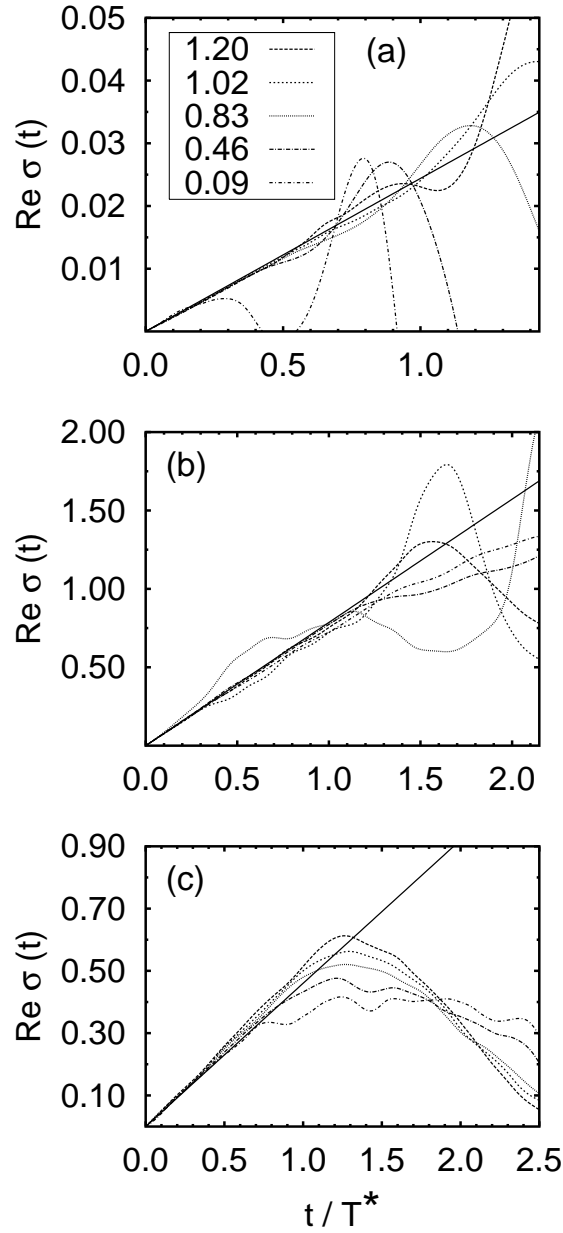
Figure 4.3: One-dimensional model Hamiltonian Eq. (4.13): Real part of $\sigma(t)$, $\mathrm{Re}\,\sigma(t)$ [Eq. (4.16)] for selected initial Gaussians. (a) model A ($g = 0.09$) levels $0\pm$, (b) model A levels $1\pm$, and (c) model B ($g = 0.17$) levels $0\pm$. The initial position x_α is indicated, the momentum p_α is zero and $\gamma_\alpha = 12.5$. The harmonic approximation to the minima of the wells yields $\gamma_{\mathrm{harm}} = 11.11$ (A) and 5.9 (B), respectively. The solid line indicates the exact linear function. The expectation value of energy with respect to the Gaussians are (largest position x first) 0.67, 0.38, 0.39, 0.80, 1.11 for model A and 1.19, 0.90, 0.91, 1.32, 1.63 for model B (in units of the barrier height). For remarks on the energy dependence: see text. (Note the different scale of the time axes.)

with initial position closer to the barrier deviate more rapidly from the exact result, while this statement is not true for Fig. 4.3b. Furthermore, there seems to be no general rule correlating the deviations and the energy of the Gaussians (cf. caption of Fig. 4.3).

4.2.2   The two-dimensional case

Application of the present quantum-semiclassical method to the important SMC Hamiltonian [cf. Eq. (3.17)] showed that the extraction of tunneling splittings is possible for a two-dimensional system, too [39]. This Section gives the interpretation of that observation based on the technique of inspecting $\sigma(t)$ developed in the previous Section [II]. The SMC parameter set $(\omega, \gamma, g) = (0.48, 0.39, 0.10)$ corresponding to malonaldehyde [30, 74] was used. Malonaldehyde has a rather large ground state tunneling splittings which facilitates its determination.

The 1D square-quartic Hamiltonian with $g = 0.10$ has two split levels below the barrier. The set of $L = 14$ Gaussians of the previous Section suffices to diagonalize these levels. A set $\{|\tilde{\Psi}_\alpha\rangle\}$ of $L = 14$ 2D Gaussians was chosen as initial wave packets. The x positions were equivalent to the 1D set $\{|\Psi_\alpha\rangle\}$ (cf. Section 4.2.1) while the the q positions were chosen in order to minimize the potential part of the SMC Hamiltonian for fixed x. The width in both directions was equivalent to the 1D case, namely $\gamma_\alpha = 12.5$.

Results obtained by numerically exact and HK propagation are compared in the following. The exact propagation was performed by using a 2D DVR grid and the short-iterative Lanczos integrator (implemented in the MCTDH package [140]). The HK propagation parameters are equivalent to the 1D case. Fig. 4.4 shows the harmonic inversion plot for exact and HK-propagation for the present SMC Hamiltonian, respectively. The definition of the characteristic time $T^* = 2\pi/g$ is adopted here. For the exact propagation the ground state level (cf. Fig. 4.4b) and the lowest excited levels (cf. Fig. 4.4a) converge before $1T^*$. A diagonalization of $\hat{H}_{\text{SMC}}$ with $L = 14$ Gaussians does not yield this accuracy.

For the HK-propagation the ground state splitting (cf. Fig. 4.4d) is present for about $2T^*$; after that time no splitting can be identified. However, the accuracy of the semiclassical ground state levels is considerably lower than in the exact case. The ground state levels appear to be shifted to higher energies and the splitting varies slowly with time; the average splitting is larger than in the exact case. The principal finding for the excited levels are similar: one observes a considerable lower accuracy and an overall shift of the levels to higher energy values.

For the evaluation of the expectation value of $\hat{P}$ (cf. Sec. 4.2.1) it is more
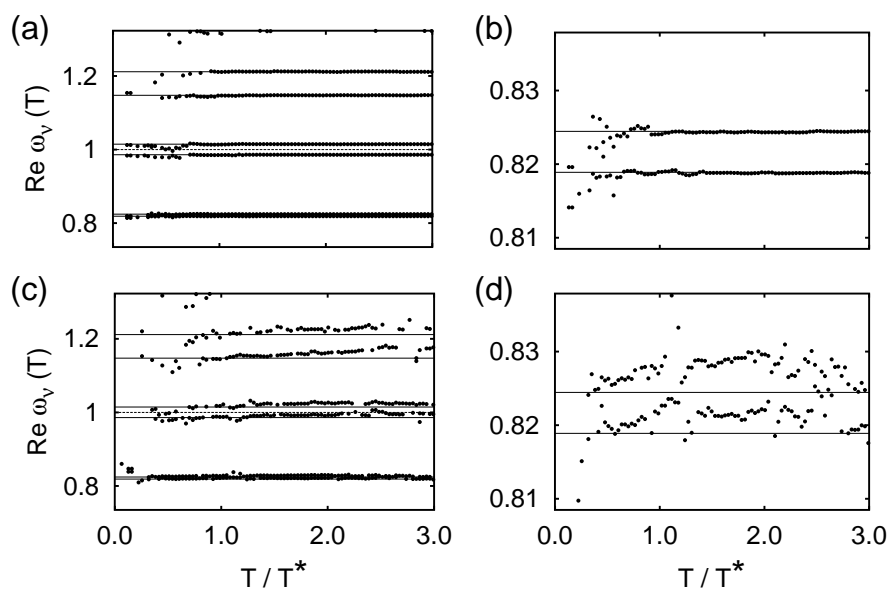
Figure 4.4: Two-dimensional SMC-Hamiltonian Eq. (3.17) with parameters for malonaldehyde $(\omega, \gamma, g) = (0.48, 0.39, 0.10)$: Frequencies $\omega_\nu(T)$ in units of the barrier height vs. propagation time T in units of T^* obtained by harmonic inversion of the 14×14 cross-correlation matrix. Upper row: exact propagation, lower row: HK-propagation, right column: ground state energy region enlarged. The FDM parameters (cf. Section 4.1.3) are $J = 3$, $\omega_{\text{center}} = 0.9$, $R_{\text{TOL}} = 10^{-4}$, $E_{\text{TOL}} = 3 \cdot 10^{-3}$, $I_{\text{TOL}} = 5 \cdot 10^{-2}$.
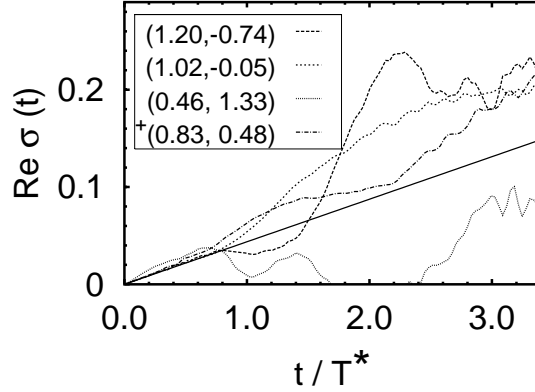
Figure 4.5: Two-dimensional SMC-Hamiltonian Eq. (3.17) with parameters for malonaldehyde $(\omega, \gamma, g) = (0.48, 0.39, 0.10)$: Real part of $\sigma(t)$ [Eq. (4.16)], $\mathrm{Re}\,\sigma(t)$, for selected initial Gaussians. The initial positions are indicated; the other parameters are $\mathbf{p} = 0$ and $\gamma = 12.5$ despite that Gaussian marked with $^+$ were the parameters are $(\gamma_x, \gamma_q) = (15.78, 4.72)$. The expectation values of the energies are (in units of the barrier height): 1.62, 1.16, 1.23, 0.91. (Remarks: see text)

convenient to express the eigenstates $|\tilde{\varphi}_\nu^\pm\rangle$ of the SMC Hamiltonian as,

$$|\tilde{\varphi}_\nu^\pm\rangle = \sum_{j_1,j_2} \tilde{c}_{\nu,j_1 j_2}^\pm |\chi_{j_1}^{(1)}\rangle |\chi_{j_2}^{(2)}\rangle, \tag{4.19}$$

where $\tilde{c}_{\nu,j_1 j_2}^\pm$ are expansion coefficients and $|\chi_{j_k}^{(k)}\rangle$ with $k = 1, 2$ are harmonic oscillator basis functions centered at $x = 0$ ($q = 0$). The basis was chosen such that the width of the ground state Gaussian equals the HK parameter γ. Then, the evaluation of matrix elements $\langle\chi_{j_1}^{(1)}|\langle\chi_{j_2}^{(2)}|\hat{K}^{(\mathrm{HK})}(t)|\Psi\rangle$ is very efficient (cf. Appendix B).

Fig. 4.5 shows $\mathrm{Re}\,\sigma(t)$ for several initial Gaussian wave packets $|\Psi\rangle$. The parameters are given in the figure caption. For the first two Gaussians shown, with initial positions $(1.2, -0.74)$ and $(1.05, -0.05)$, $\mathrm{Re}\,\sigma(t)$ increases linearly until $0.8T^*$; for proceeding time the deviations from a linear increasing is evident. $\mathrm{Re}\,\sigma(t)$ of the third Gaussian with initial position $(0.46, 1.33)$ deviates from the exact straight line right from the beginning, stays approximately linear until $0.7T^*$, and shows a more prominent deviation for proceeding time. The result for the fourth Gaussian with initial position $(0.83, 0.48)$ shows a linear increase up to $0.5T^*$. The energy of this Gaussian is below the barrier (cf. caption of Fig. 4.5 for energies of the Gaussians), a property which was achieved by changing the parameters of the Gaussian to $(\gamma_x, \gamma_q) = (15.78, 4.72)$. There is no significant correlation between deviation from the exact result and energies above or below
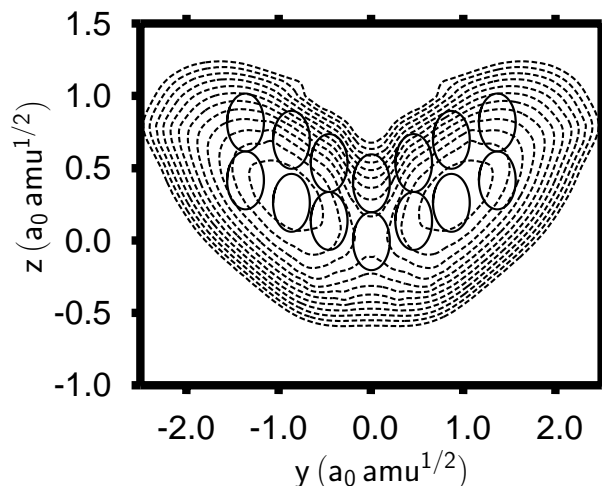
Figure 4.6: Contour plot of the two-dimensional potential $V(y, z)$ of 3,7-dichlorotropolone (see text for details of the quantum chemistry calculations). The coordinates (y, z) describe the hydrogen position in the molecular plane relative to the transition state. The remaining DOF are relaxed; the zero-point energy is included (cf. Sec. 5.2). The contour line-spacing is $500 \, \text{cm}^{-1}$. The barrier height is $1822 \, \text{cm}^{-1}$. Positions of the Gaussians are indicated; the other parameters are $\gamma_\alpha = 12.5$ and $p_\alpha = 0$ (in a.u.).

the barrier. The findings are reminiscent of the 1D case shown in Fig. 4.3: the actual deviation from the exact result depends on the initial Gaussian as well as on the propagation time. In the 2D case the strong deviations from the exact result for times larger than the characteristic period T^* is evident and can be interpreted as a corresponding change in the effective Hamiltonian $\hat{H}'$ of the HK-propagator.

Concerning the ground state, that is clearly split by tunneling, comparison of Fig. 4.4 and 4.5 shows that the time interval for which a tunneling splitting can be obtained is not much larger than the time for which there are split eigenvalues in the effective Hamiltonian. This is reminicent of the 1D case discussed before. Moreover, FDM relies on the full time interval $[0, T]$. This explains why the splitting can be obtained when there is already a strong deviation from linear behavior for some Gaussians in Fig. 4.5. The present finding suggest, that FDM extracts tunneling splittings from the *effective* Hamiltonian. This is in contrast to the notion of a quantum-semiclassical method [36]. In fact, FDM combined with semiclassical propagation is a pure semiclassical method.

There are anharmonic terms proportional to x^4 and $x^2 q$ in the SMC-PES. For the one-dimensional case the x^4-term leads to a constant energy shift of the effective Hamiltonian for $t \rightarrow 0$. The 2D error is not known analytically. However, the one-dimensional findings suggest that the semiclassical error becomes more pronounced for higher anharmonic terms. For instance, a x^5-term leads to an error
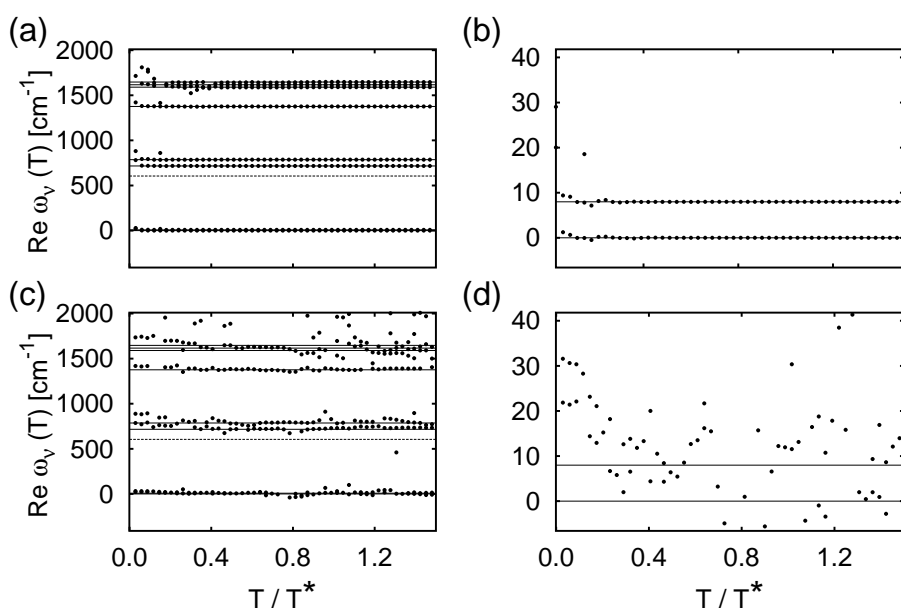
Figure 4.7: Same as Fig. 4.4 but for a 2D model for the 3,7-dichlorotropolone tautomerization (cf. Fig. 4.6). The FDM parameters are $J = 5$, $\omega_{\text{center}} = 800\text{cm}^{-1}$, $R_{\text{TOL}} = 10^{-6}$, $E_{\text{TOL}} = 80\text{cm}^{-1}$, $I_{\text{TOL}} = 10^{-1}$.

operator that is proportional to the position operator at $t = 0$, i.e., there appears an unphysical additional linear term in the effective PES. Higher order anharmonic terms are likely to appear in a realistic PES that is constructed *ab-initio* by employing modern quantum chemistry techniques. For instance, consider the 2D PES for the tautomerization reaction of 3,7-dichlorotropolone shown in Fig. 4.6. The coordinates (y, z) refer to the position of the reactive hydrogen in the molecular plane. The PES was obtained by Gaussian 98 [124] using the DFT method (B3LYP functional) and the 6-31+G(d,p) basis set [141]. For fixed (y, z), the remaining DOF were relaxed [141] and the zero-point energy was included (cf. Sec. 5.2). Here, the PES serves as an example for a realistic model (concerning the anharmonicities).

The parameters of the initial Gaussians (cf. figure caption of Fig. 4.6) were manually optimized in order to minimize the necessary propagation time for convergence of the lowest levels. Two of the Gaussians were placed near the minima and the others were placed along a straight line connecting the minimum and transition state. The width was chosen similar to the width of a ground state wave packet. A set of $L = 14$ Gaussians was sufficient for that purpose. The number of sampled trajectories per propagated wave packet was $1 \cdot 10^6$; the integrator step-size was $0.2\,\text{fs}$. The numerical exact propagation was performed by using a short-iterative Lanczos scheme with a DVR grid [140].

The FDM results for the exact and HK-propagated cross-correlation matrices, respectively, are shown in Fig. 4.7. The time is given in units of the period $T^* = \hbar\pi/E_{\text{ZPE}} = 13.3\,\text{fs}$ with zero-point energy E_{ZPE}. For the exact propagation, the ground state levels $0+$ and $0-$ (cf. Fig. 4.7b) converge within $0.3T^*$. The lowest excited levels (cf. 4.7a) converge within $0.3 - 0.5T^*$; even the three close lying levels above $1500\,\text{cm}^{-1}$ are resolved. For the HK-propagation, the ground state levels (cf. Fig. 4.7d) do not converge to the exact result. One finds a number of frequencies scattered in the vicinity of the exact levels, but no splitting appears. Figure 4.7c shows similar findings for the excited levels: while there are frequencies scattered around the exact levels, the splitting of the first excited level and the splitting of the three levels above 1500 cm^{-1} cannot be resolved. The accuracy of the semiclassical results is poor in comparison with the exact result. The reason for the large deviation from the exact result is clearly the increased anharmonicity of the potential. Due to this anharmonicity, $\hat{H}_{\text{eff}}$ (cf. Sec. 4.1.2) does not only deviate from $\hat{H}$ for $t = 0$ but does also exhibit a fast deviation from the exact Hamiltonian with increasing time. Although the exact result converges within less than T^* this period seems to be too large for an accurate semiclassical extraction of the tunneling splitting using the present set of Gaussians. Note, in order to identify spurious eigenvalues, the determined energy levels must be stable for times of the order of the characteristic period.

Apparently, the amount of (systematic) noise in the HK-propagated cross-correlation matrix is much higher than that in the cross-correlation matrices of the simple models that were discussed before. Nevertheless, the ground state energy in units of the absolute barrier height is 0.67, a value that is intermediate between those considered in the one-dimensional model A and B and the two-dimensional SMC model, respectively. Therefore, taking this as a simple measure, the different systems should be comparable. Due to the high amount of noise, a change of R_{TOL} may have a significant influence on the semiclassical spectrum. This is similar to the analysis of noisy experimental data, a topic that takes considerable attention in applications of the FDM [38]. The semiclassical spectrum for different values of R_{TOL} is shown in Fig. 4.8. For R_{TOL} larger than 10^{-6} the splitting of the ground and first excited state gets stabilized. The finding suggests that tunneling is present in the effective Hamiltonian, but splittings cannot be reliably predicted.

4.2.3   Conclusion

It was supposed that the action of the Herman-Kluk propagator $\hat{K}^{(\text{HK})}$ is governed by an effective (generally non-Hermintian and time-dependent) Hamiltonian $\hat{H}_{\text{eff},t}$, $\hat{K}^{(\text{HK})} \approx \exp\{-i\,\hat{H}_{\text{eff},t}\,t/\hbar\}$ [36]. Ankerhold *et al.* [98] showed, for
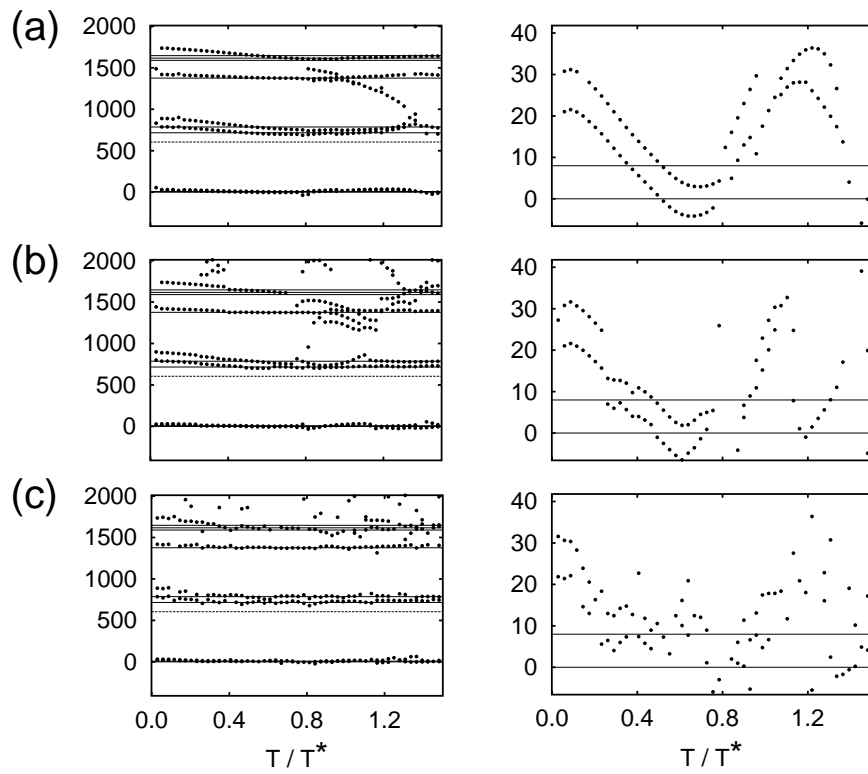
Figure 4.8: Semiclassical levels obtained by FDM. Same as Fig. 4.7, but for different parameters R_{TOL} of the SVD. (a) $R_{\mathrm{TOL}} = 10^{-2}$ (b) $R_{\mathrm{TOL}} = 10^{-3}$ (c) $R_{\mathrm{TOL}} = 10^{-8}$.

the one-dimensional case, that $\hat{H}_{\mathrm{eff},t}$ is generally different from the exact quantum Hamiltonian $\hat{H}$. Yet $\hat{H}_{\mathrm{eff},t}$ may involve tunneling. For instance, for $t = 0$ it differs from the square-quartic Hamiltonian only by a constant (cf. Section 4.2.1).

It was shown in Ref. [39] for one- and two-dimensional model potentials that tunneling splittings can be obtained by the combination of HK propagation and harmonic inversion of cross-correlation functions for multiple Gaussians (quantum-semiclassical approach). This was attributed to the assumed quantum aspect that is introduced in a semiclassical propagation by using more than one wave packet. (For an infinite number of wave packets this refers to a diagonalization.) It was suggested, that distributing Gaussians along DOF for which tunneling is important may lead to an efficient combination of quantum and semiclassical techniques (quantum-semiclassical approach). However, the present study suggest that the quantum effect 'tunneling' is not introduced by the set of Gaussians, because split energy levels are present for short times in $\hat{H}_{\mathrm{eff},t}$. This renders the view of a quantum semiclassical method [36] unsound. In particular, even for a complete basis the effective Hamiltonian at $t = 0$, $\hat{H}_{\mathrm{eff},0}$, - instead of the quantum Hamiltonian $\hat{H}$ - is diagonalized.

It is known that semiclassical results concerning non-classical effect may depend upon so-called *arbitrary parameters* [134, 133, 132]. For instance, the set of Gaussians used for the square-quartic Hamiltonian was chosen to diagonalize the low lying eigenlevels, but infinitely many (even non-Gaussian) basis sets do diagonalize these levels within the same accuracy. Quantum mechanically, the actual choice is irrelevant as long as only the same low lying levels are concerned. However, for a HK propagation certain basis set may be superior compared to the one used. This can be illustrated by re-inspection of Fig. 4.3 or Fig. 4.5: the time-interval for which $\mathrm{Re}\,\sigma(t)$ is almost linear depends on the initial conditions of the Gaussian. (This is reminiscent of the findings in Ref. [133], for instance.) The choice of an optimized set would mean to decrease the influence of the error operator on the HK propagation (cf. Sec. 2.3.2). The error operator, however, is generally unknown. Thus, the present method has the same drawbacks as any other semiclassical method. In particular, semiclassical eigenenergies may be obtained for rather large systems but quantum effects cannot be introduced simply by adding enough Gaussians.